Geometrized dynamics and search of structural instabilities in SU(2) models

D. M. Jezek and E. S. Hernández
Departamento de Física, Facultad de Ciencias Exactas y Naturales, Universidad de Buenos Aires, 1428 Buenos Aires, Argentina
(Received 24 March 1986)

The structural instabilities or general nonthermodynamic phase transitions of the time-dependent Hartree-Fock flow on the Bloch sphere are investigated for different SU(2) model Hamiltonians by means of a simple geometrical construction. In particular, the generalized Lipkin-Meshkov-Glick model is found to exhibit a variety of instabilities, opposite to the standard Lipkin-Meshkov-Glick model which possesses only one ground-state (thermodynamic) phase transition. The relationship between the fixed points of the time-dependent Hartree-Fock flow and the tangency points between energy surfaces and the Bloch sphere is established. It is found that different Hamiltonians of the class under study give rise to flow patterns whose invariant sets may contain either rotations or librations, which in turn may be degenerate as well as nondegenerate, in contrast to previously investigated models.

I. INTRODUCTION

The models for structural and dynamical features of many-body systems based on Hamiltonians that commute with the Casimir operator of a Lie algebra have deserved attention in nuclear physics.[1–8] In particular, a two-level model for fermions interacting via a monopole-monopole force originally proposed by Lipkin, Meshkov, and Glick[1] (LMG) can be formulated with exclusive resort to the generators of an SU(2) algebra. This property made room, on one hand, for the classification of the spectrum of the system with respect to the irreducible representations of the rotation group,[1] and on the other, to the establishment of a Hamiltonian flow on a compact Grassmann manifold—the Bloch sphere—as the manifestation of the mean field dynamics arising from the time-dependent-Hartree-Fock (TDHF) procedure.[9]

The self-consistent phase diagram of the so-called standard LMG model has been investigated by Kan *et al.*,[9] and several authors have contributed as well to clarifying this interesting problem from several viewpoints.[10–19] Departures between the TDHF and the exact dynamics have been ascribed to the fact that the former gives rise to two degenerate regions with local trajectories in phase space,[17,18] and an alternative approach to a mean field description of the motion has been proposed[18] with good perspectives. Since the appearance of degenerate invariant sets in phase space is related to the parity symmetry of the standard LMG Hamiltonian, a challenging task has been the study of an SU(2) model for which such a symmetry has been suppressed.[19] The present work aims at an investigation of the TDHF evolution undergone by model systems with SU(2) Hamiltonians that combine the features of both the standard and the generalized LMG models with those of the parity-nonconserving model of Ref. 19.

For this purpose, in Sec. II we present an SU(2) Hamiltonian that contains a parity conserving and a parity-nonconserving interaction and express the TDHF equations of motion as a vector Euler equation for the expectation value of the quasispin vector operator. It is then seen that the collective trajectories of the TDHF flow are obtained from a simple geometric construction. This viewpoint allows for a qualitative inspection and characterization of structural instabilities of the phase flow—catastrophes—that is extensively illustrated in Sec. III for the general LMG model. Both the orbits on the Bloch sphere and in the TDHF phase space are provided, the latter being just mappings of the former. In Sec. IV, the parity nonconserving interaction is introduced and it is seen that the effects of symmetry breaking manifest themselves as the appearance of a set of orbits not present in the former situation, i.e., nondegenerate librations. Some exact calculations and their relation to the TDHF flow are shown in Sec. V. Finally, the summary and conclusions are presented in Sec. VI.

II. TDHF DYNAMICS OF THE QUASISPIN VECTOR FOR THE GENERAL SU(2) HAMILTONIAN

On the grounds of a two-level model with spacing ϵ for a many-fermion system with $N=2$ J particles, one usually introduces a quasispin vector operator $\hat{\mathbf{J}}$ whose components yield a basis for an SU(2) algebra.[1–19] In order to test some method in many-body physics, devised for either structural or dynamical investigations, one then proposes a Hamiltonian $\hat{H}(\hat{\mathbf{J}})$ that commutes with the Casimir operator $\hat{\mathbf{J}}\cdot\hat{\mathbf{J}}$, whose spectrum consequently lies on the irreducible representations of the SU(2) group. In this work, we choose the Hamiltonian,

$$\hat{H}=\epsilon\hat{J}_z+\frac{V}{2}(\hat{J}_+^2+\hat{J}_-^2)+\frac{W}{2}\{\hat{J}_+\hat{J}_-\}+\frac{U}{2}(\{\hat{J}_+\hat{J}_z\}+\{\hat{J}_-\hat{J}_z\}), \tag{2.1}$$

where the curly braces denote the anticommutator. This Hamiltonian belongs to a class that extends the one originally proposed by Abecasis, Faessler, and Plastino[20] (the AFP model) to generalize in a nontrivial fashion the tradi-

tional LMG Hamiltonian[1] (corresponding to an interaction strength $U=0$) so as to allow for one-particle—one-hole excitations. The most important feature of the AFP Hamiltonian is its parity-nonconserving character,[21] and recently, the TDHF dynamics for the case $V=W=0$ was examined.[19]

For the current study we have decided to work in the space of the q numbers $\langle\hat{\mathbf{J}}\rangle=\mathbf{J}$ instead of the phase space,[9,12,13,17,18] since the geometry of the orbits can be more straightforwardly described in the former. Indeed, the motion of the so-called polarization vector $\mathbf{J}$ is given by a vector expression, independent of the system of coordinates. This fact presents us with two additional advantages: On one hand, we may be able, in a number of situations, to find more convenient canonical coordinates than the traditional ones;[9,12,13,17,18] on the other hand, in $\mathbf{J}$ space one is prevented from encountering spurious singularities such as those associated with mapping the poles of the Bloch sphere on the (q,p) plane,[9,17–19] where $q=\tan^{-1}(J_x/J_y)$ and $p=J_z$.

As far as TDHF dynamics is concerned, it is well established that it is a variational dynamics on a manifold of coherent states—the Bloch sphere.[22,23] It is easy to show, resorting to disentangling formulae,[22] that on such a manifold, the expectation value of a two-fermion operator built out from the quasispin factorizes as

$$\langle\tau|\tfrac{1}{2}\{\hat{J}_i,\hat{J}_j\}|\tau\rangle=\frac{N-1}{N}J_iJ_j+\frac{N}{4}\delta_{ij} \tag{2.2}$$

for $i,j=x,y,z$. With this prescription, we obtain, for the model Hamiltonian (2.1), a TDHF Hamiltonian,

$$\epsilon^{-1}H_{\mathrm{TDHF}}=\epsilon^{-1}\langle\tau|\hat{H}|\tau\rangle =J_z+\frac{1}{2J}\chi_+J_x^2+\frac{1}{2J}\chi_-J_y^2+\frac{\chi}{J}J_xJ_z+\frac{WJ}{\epsilon}\ , \tag{2.3}$$

with the mean field strengths

$$\chi_\pm=\frac{N-1}{\epsilon}(W\pm V)\ , \tag{2.4a}$$

$$\chi=\frac{N-1}{\epsilon}U\ . \tag{2.4b}$$

It is clearly seen that Eq. (2.3) defines a family of quadrics, whose intersections with the Bloch sphere determine the TDHF orbits. On the other hand, these orbits are the locus of the polarization vector whose motion is given by Ehrenfest's theorem,

$$i\frac{d\mathbf{J}}{dt}=\langle\tau|[\hat{\mathbf{J}},\hat{H}]|\tau\rangle\ . \tag{2.5}$$

One should notice that the model Hamiltonian is of the form

$$\hat{H}=\boldsymbol{\Omega}\cdot\hat{\mathbf{J}}+\tfrac{1}{2}\hat{\mathbf{J}}\,\vec{\alpha}\,\hat{\mathbf{J}}\ , \tag{2.6}$$

with $\vec{\alpha}$ a symmetric matrix. Angular momentum commutation rules then yield

$$\frac{d}{dt}J_i=\epsilon_{ijk}\Omega_jJ_k+\tfrac{1}{2}\alpha_{jk}\epsilon_{ikl}\langle\{\hat{J}_j,\hat{J}_l\}\rangle\ , \tag{2.7}$$

whatever the reference state $|\ \rangle$. In Eq. (2.7), the symbol ϵ_{ijk} denotes the totally antisymmetrized tensor. Now, according to Eq. (2.2) we have on the Bloch sphere

$$\frac{d}{dt}J_i=\epsilon_{ijk}\Omega_jJ_k+\alpha_{jk}\frac{N-1}{N}J_j\epsilon_{ikl}J_l =\epsilon_{ijk}\left[\Omega_j+\alpha_{lj}\frac{N-1}{N}J_l\right]J_k \tag{2.8}$$

that can be written in an abridged way as a vector formula,

$$\frac{d}{dt}\mathbf{J}=\nabla_JH_{\mathrm{TDHF}}\times\mathbf{J} \tag{2.9}$$

if we agree on an extension of expression (2.3), otherwise valid just on the Grassmann manifold, to the full $\mathbf{J}$ space. It becomes then clear that whenever the interaction matrix $\vec{\alpha}$ is different from zero, the TDHF dynamics (2.8) and the exact one (2.5) coincide if and only if the polarization vector touches the Bloch sphere.

For the Hamiltonian under consideration, Eq. (2.8) then yields the system

$$\epsilon^{-1}\frac{dJ_x}{dt}=-J_y\left[1-\frac{\chi_-}{J}J_z\right]-\frac{\chi}{J}J_xJ_y\ , \tag{2.10a}$$

$$\epsilon^{-1}\frac{dJ_y}{dt}=J_x\left[1-\frac{\chi_+}{J}J_z\right]+\frac{\chi}{J}(J_x^2-J_z^2)\ , \tag{2.10b}$$

$$\epsilon^{-1}\frac{dJ_z}{dt}=(\chi_+-\chi_-)J_xJ_y+\chi J_yJ_z\ . \tag{2.10c}$$

III. THE TDHF ENERGY SURFACES AND ORBITS OF THE GENERAL LMG MODEL

As quoted in the preceding section, the LMG Hamiltonian arises from (2.1) when the interaction strength U vanishes. For the sake of limiting the possibilities that may appear, we will restrict ourselves to positive parameters V and W, implying $\chi_+>0$, both in this and in the following section. We then consider three cases, according to whether χ_- is equal to, larger than, or smaller than zero.

A. $\chi_-=0$

In this case the quadrics (2.3) are parabolic cylinders, their axis aligned with the direction J_y. If $\chi_+<1$, the curvature of the parabolas on the (J_x,J_z) plane at the north pole is smaller than $1/J$, the curvature of the sphere. Accordingly, the intersections are single curves linking the J_z axis, and the phase diagram exhibits only rotations. The north (south) pole corresponds to an absolute energy maximum (minimum), and no orbit degeneration exists. This situation is illustrated in Fig. 1, where the trajectories of the TDHF polarization vector on the Bloch sphere and the corresponding phase diagram are displayed for $\chi_+=0.5$.

When χ_+ reaches the value unity, a phase instability takes place, since the curvature of the parabola at the north pole equals that of the sphere. Higher values of χ_+

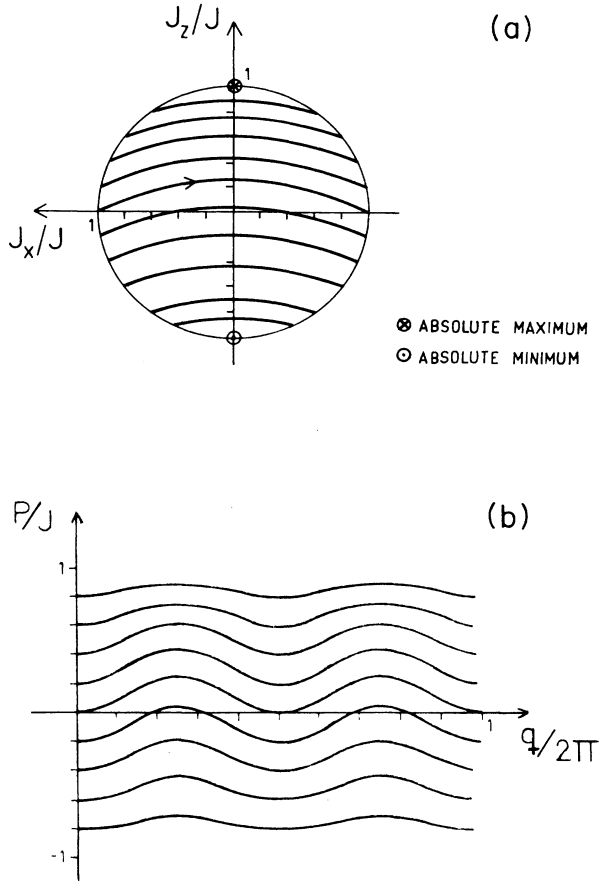

FIG. 1. The trajectories of the TDHF polarization vector on the Bloch sphere (a) and the corresponding phase diagram (b) for the selection $\chi=\chi_-=0,\chi_+=0.5$. The arrow in part (a) indicates the direction of the velocity $\dot{\mathbf{J}}$. The axes follow the usual right-hand convention, i.e., the J_y axis is an outgoing one.

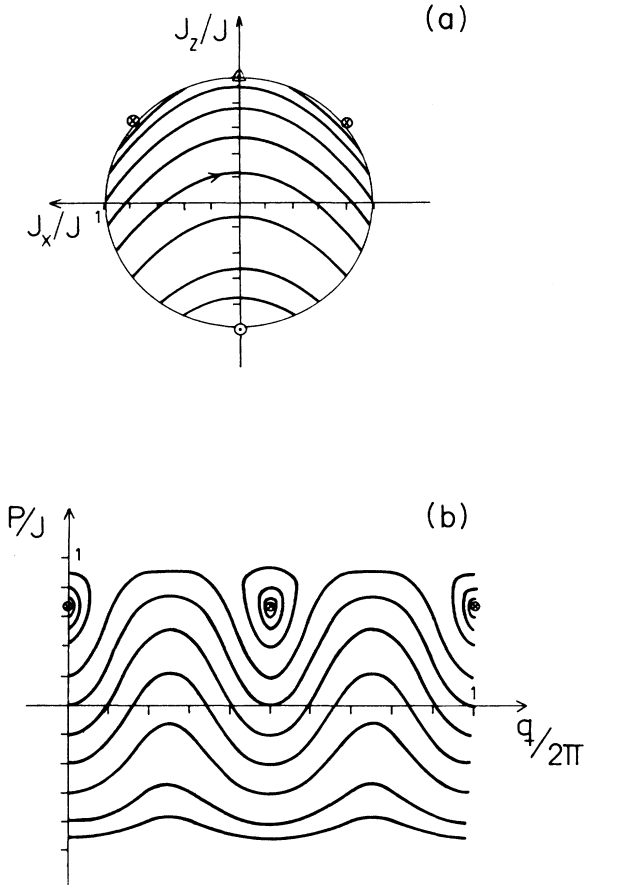

FIG. 2. Same as in Fig. 1 but for an interaction strength $\chi_+=1.5$. It is seen that the elliptical point at the north pole in Fig. 1 has undergone a pitchforklike bifurcation into a saddle and two symmetric elliptic points.

determine that those energy surfaces with their vertices at any location J_z such that $J<J_z<J\,(1+\chi_+)/2$ intersect the sphere twice. This fact gives rise to two sets of orbits, symmetrically located and energetically degenerated, that do not link the J_z axis and represent local oscillations or librations. This is illustrated in Fig. 2 for $\chi_+=1.5$. In this case, two absolute (identical) maxima appear with coordinates $(J/\chi_+)(\pm(\chi_+^2-1)^{1/2},0,1)$ in **J** space.

For strong interactions $\chi_+\gg 1$, the TDHF Hamiltonian reads

$$H_{\mathrm{TDHF}}\sim\frac{\epsilon}{2J}\chi_+J_x^2\ , \tag{3.1}$$

indicating that the energy surfaces are essentially planes lying parallel to the (J_y,J_z) one. Notice that although the expression of the TDHF Hamiltonian is very simple in quasispin representation, it becomes more involved in the (q,p) coordinates (cf. Sec. II for the relationship between J and q,p). In this case, however, a proper selection of canonical coordinates is $p'=J_x$ and q' equal to the axial angle with respect to the J_x axis. Any possible motion is just a rotation around this axis with a period

$$T_{\mathrm{TDHF}}=\frac{2\pi}{\dot{q}'}=\frac{2\pi J}{\epsilon\chi_+p'}\ . \tag{3.2}$$

B. $\chi_-<0$

In this range of interaction parameters ($V>W$) the quadrics are one-sheet hyperboloids. Kan *et al.*[9] investigated the phase diagram in the case $W=0$ that constitutes the most popular version of the LMG model. In this case, $\chi_+=-\chi_-$, and the eigenvalues of the quadrics are identical. When the common value $|\chi_\pm|$ is less than unity, only rotations occur. When $\chi_+=1$ ($\chi_-=-1$), a phase transition occurs, consisting of a simultaneous departure of both absolute extrema from the poles and the appearance of degenerate librations centered at the elliptic points $(J/\chi_+)(\pm(\chi_+^2-1)^{1/2},0,1)$ and $(J/|\chi_-|)(0,\pm(\chi^2-1)^{1/2},-1)$ at the northern and southern hemispheres, respectively. This degeneracy can be viewed, on a geometrical basis, as a consequence of the fact that the vertex of the hyperboloid lies off the sphere on the J_z axis; one can realize as well that the energy maxima at the northern

hemisphere correspond, for given χ_+, to those points where a quadric becomes tangent to the sphere. The same happens when χ_+ is different from χ_-, and can be appreciated in Fig. 3 for $\chi_+=2$ and $\chi_-=-1.5$, where it is clearly visualized that the maxima and minima are not symmetrically located with respect to the equator as in the case examined in Ref. 9. In the present case, two different phase transitions have taken place, one for $\chi_-=-1$ affecting the south pole, the other for $\chi_+=1$ involving the north pole.

C. $\chi_->0$

The family of quadrics consists of a set of elliptic paraboloids. When both χ_+ and χ_- are smaller than unity, only rotations can take place. When $\chi_+=1$ for $\chi_-<1$, a bifurcation occurs that splits the maximum at the north pole into two degenerate elliptic points at the location $(J/\chi_+)(\pm(\chi_+^2-1)^{1/2},0,1)$. If, moreover, χ_- increases

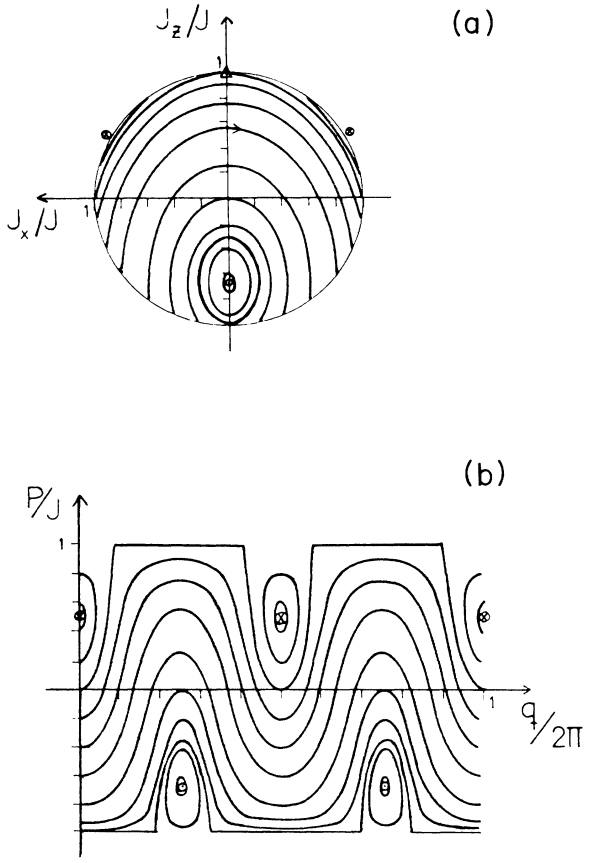

FIG. 3. Same as in the preceding figures for $\chi=0$, $\chi_+=2$, and $\chi_-=-1.5$. It is seen that the elliptic point at the south pole in Figs. 1 and 2 has undergone a pitchforklike bifurcation into a saddle and two elliptic points. Only the elliptic point located "in front" of the sphere is drawn. Notice that the separatrices going from the equator through the north pole or around the elliptic points through the south pole are mapped on curves with slope discontinuities in phase space. The latter is nothing but a convention to express the continuity of such trajectories and simply puts into evidence the impossibility of mapping a sphere on a plane.

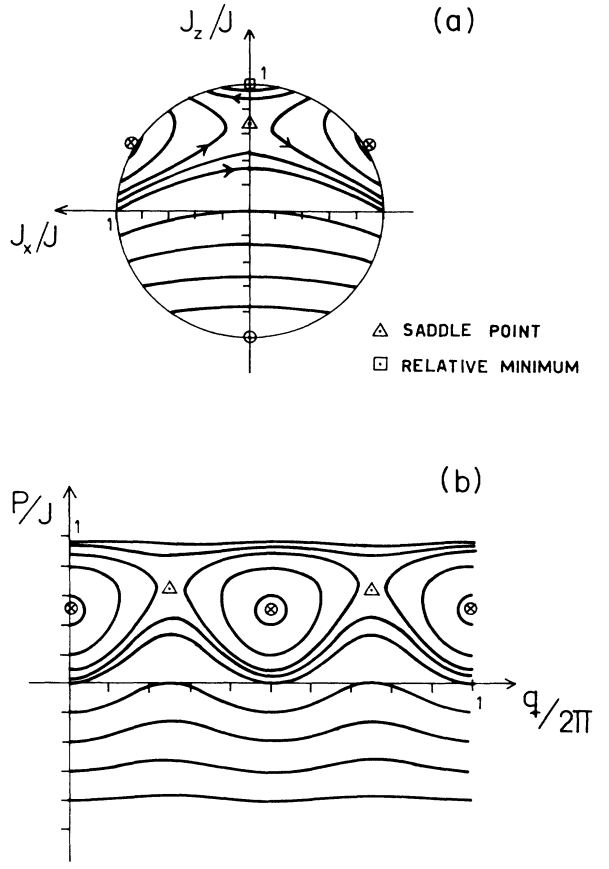

FIG. 4. Same as in the preceding figures for $\chi=0$, $\chi_+=2$, and $\chi_-=1.5$.

while keeping $\chi_-<\chi_+$ and the latter at a value above unity, a second instability occurs that creates two rotation zones. This is illustrated in Fig. 4 for $\chi_+=2,\chi_-=1.5$, where one can appreciate the presence of two hyperbolic points on the (J_y,J_z) plane with ordinate $J_z=J/\chi_-$. In this case, the north (south) pole is a relative (absolute) minimum. Since there exist now two saddle points lying between the two rotation regions, the orbits closer to the north pole possess degenerate partners below the separatrices.

If $\chi_+=\chi_-$ the quadrics become circular paraboloids and the phase diagram presents horizontal lines, degenerate on both sides of the circumference $J_z=J/\chi_+$ if $\chi_\pm>1$, where the quadric is tangent to the sphere. Any orbit has a period $T=2\pi/\epsilon(J-\chi_+J_z)$. It is worth noticing that in this case the circumference $J_z=J/\chi_+$ consists of energy maxima, each point being thus a fixed point. In other words, the maximum is a line rather than a single point as in the examples discussed above. In addition, all energies in the interval $\epsilon J[1,(\chi_++1)/2]$ are degenerate.

IV. THE TDHF ENERGY SURFACES AND ORBITS OF THE SYMMETRY-BREAKING HAMILTONIAN

In a previous work[19] we presented a discussion of the TDHF phase portrait of the Hamiltonian (2.1) with

$V=W=0$. In this case, the quadrics are two-sheet hyperbolic cylinders bearing the J_y axis as a degeneracy axis. In the most general case with nonvanishing V,W parameters, the eigenvalues λ and eigenvectors $\mathbf{v}$ of the quadrics read,

$$\lambda_0=\chi_-,\quad \mathbf{v}_0=(0,1,0)\ , \tag{4.1a}$$

$$\lambda_\pm=\chi[m\pm(m^2+1)^{1/2}],\quad \mathbf{v}_\pm=\left[\frac{\lambda_\pm}{\chi},0,1\right]\ , \tag{4.1b}$$

with $m=\chi_+/2\chi$. One realizes that if the three interaction strengths χ_+, χ_-, and χ are simultaneously considered, a variety of quadrics appear according to the many different ways of ordering these parameters and selecting their signs. Far from making an attempt to classify the various possibilities, we would rather discuss in detail a pair of examples so as to draw attention to the richness of flows one has at hand. We will restrict ourselves to the choice $\chi_-=0$, since in this case the J_y axis is a translation axis. Furthermore, this means $V=W$, so we are disturbing the flow in Sec. III A; Fig. 5 illustrates the deformation experienced by the flow in Fig. 1 when $\chi=\chi_+$, and we can visualize it as a departure of the absolute extrema from the poles. In contrast to the situation discussed in Ref. 19, where the parameter χ_+ vanished, these extrema are not symmetrically located with respect to the equator.

One may establish the equations for the asymptotic planes of these quadrics that read

$$\chi_+/2\cdot J_x+\chi J_z=\chi_+/2\chi\ , \tag{4.2a}$$

$$J_x=-J/\chi\ . \tag{4.2b}$$

When either asymptotic plane intersects the sphere, the phase portrait undergoes a splitting of one into two invariant regions with different curvature of the trajectories. This situation can be appreciated in Fig. 6, where both planes have penetrated the Grassmann manifold and three sets of librations and two sets of rotations can be identified. Such a figure is obtained for $\chi_+=1.5$ and $\chi=2.5$; one could regard it as a disturbance of the flow in Ref. 19 provoked by an interaction with strength χ_+, whose effect is to lift an asymptotic plane lying at the equator to the position described by Eq. (4.2a). However, in this case the axis of the hyperbolic cylinder lies outside the sphere, its coordinates being $J(-1/\chi,\chi_+/\chi)$ in the (J_x,J_z) plane. If one changes the parameters—for instance, decreasing the value of χ_+—so as to bring the axis onto the sphere, a new transition may take place since this tangency point is a saddle. Further decrease of χ_+ causes the saddle point to bifurcate into two hyperbolic points, one in front and the other behind the sphere, and a set of librations appears around a relative minimum. The corresponding phase

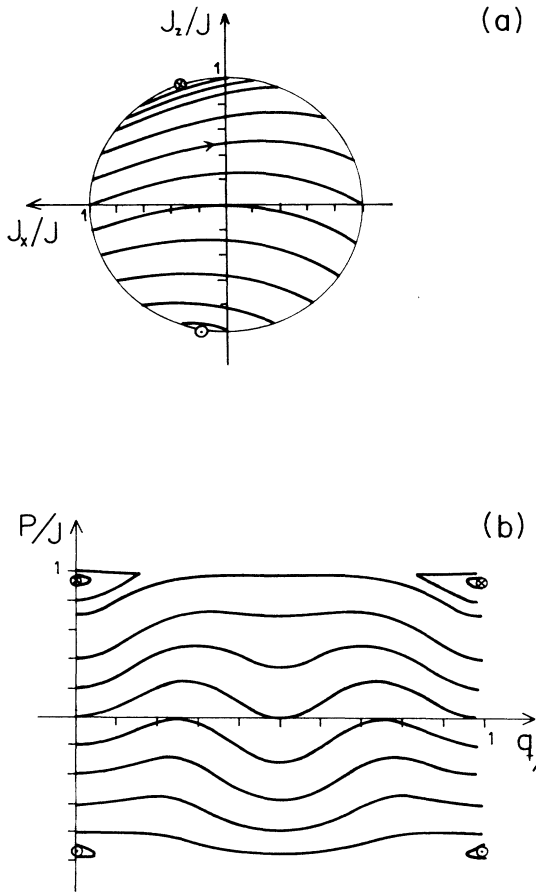

FIG. 5. Same as in Fig. 1 with $\chi=\chi_+,\chi_-=0$.

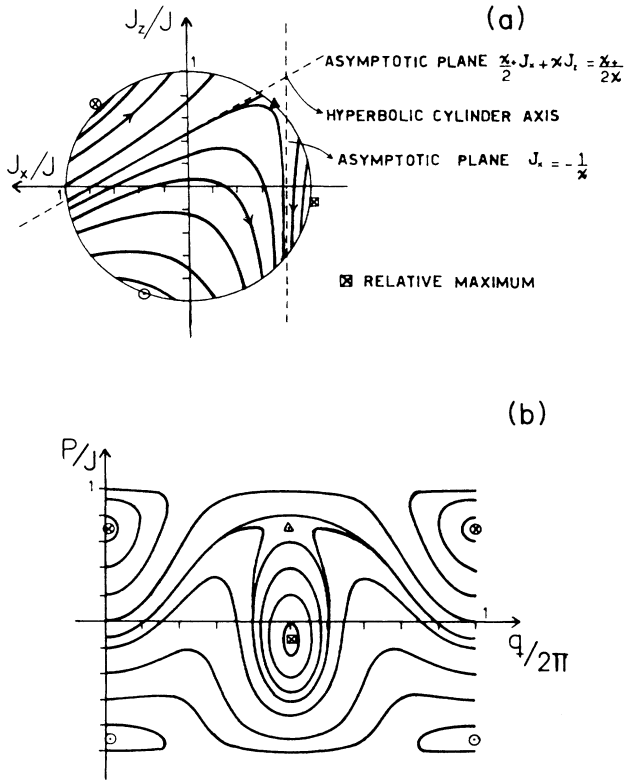

FIG. 6. Same as in the preceding figures for $\chi_+=1.5$ and $\chi=2.5$ ($\chi_-=0$). A saddle point appears at the tangency point between the sphere and a hyperbola branch.

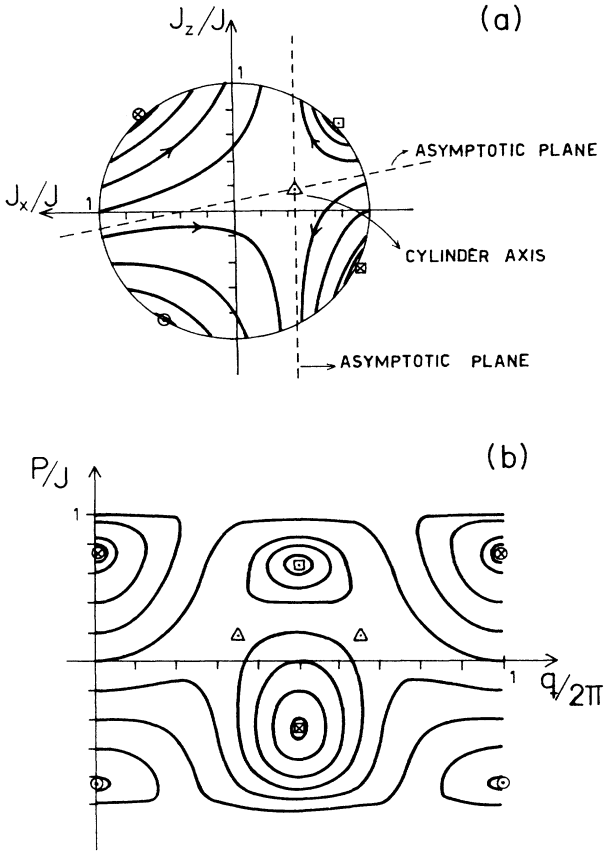

FIG. 7. Same as in the preceding figures for $\chi_+=1$, $\chi=2.3$ ($\chi_-=0$). In this case the saddle point in Fig. 6 has bifurcated into one elliptic and two saddle points.

portrait is displayed in Fig. 7 for $\chi_+=1,\chi=2.3$. In this case, both asymptotic planes become separatrices, and all possible combinations of orbits show up, namely, degenerate rotations, degenerate librations, as well as nondegenerate rotations and librations. Notice that previous to this instability the period of the orbit on the vertical plane defined by (4.2b) is finite and easily computable as

$$T=2\pi/\epsilon\{1/[(\chi_+/\chi)^2-(\chi^2-1)]^{1/2}\} .$$

V. THE EXACT POLARIZATION

If one randomly chooses a set of initial conditions, it appears that the exact polarization vector may draw regular and artistic geometric patterns. It is not our purpose in this work to carry out a detailed systematics of the many beautiful landscapes that may appear when one exactly solves the Schrödinger equation in the Dicke basis for the Hamiltonian (2.1). The enormous number of possible classifications according to the location of the initial conditions on the Bloch sphere—so as to determine the time scale within which the TDHF dynamics approaches the exact one—makes this task a piece of work in itself that is not our interest here. Indeed, up to now we mainly intended to call the reader's attention to the fact that TDHF flow patterns in SU(2) models mean a far from exhausted field of research. In this respect, this section points in an equivalent direction since it will be devoted to illustrating the richness and variety of the polarization trajectories that may appear.

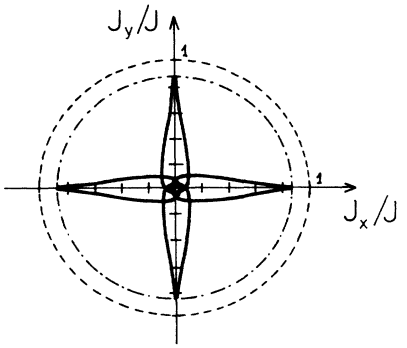

FIG. 8. The (J_x,J_y) section of a trajectory starting at a maximum of the TDHF flow pattern for $\chi=0$ and $\chi_+=\chi_-=2$.

We simply quote here three examples, all of them corresponding to the selection $\chi_+=\chi_-=2$ and $\chi=0$ for the interaction parameters. We remind the reader that in this case, the energy quadrics are circular paraboloids and the TDHF orbits are rotations, with a circle of fixed points—maxima—lying on the plane at $J_z=J/\chi_+$. It is then clear that the expectation value of the projection J_z is a constant of the motion for both dynamics. Furthermore, rotations on different half-spaces with respect to that plane may be degenerate. If one solves the Schrödinger equation and evaluates the expectation value of the quasispin operator as a function of time, sections of the exact orbit on the coordinate planes of quasispin space can be designed. Figure 8 displays the (J_x,J_y) section of a trajectory starting at a maximum with coordinates $J((\chi_+^2-1)^{1/2},0,1)/\chi_+$. It appears that the beautiful periodic, symmetric pattern shown here is far from a fixed point. One realizes that, since for the given initial condition the velocity component tangent to the Bloch sphere strictly vanishes at $t=0$, this origin of the motion is necessarily either a cuspidal or a fixed point. The former has evidently been the choice of the system under consideration.

Two degenerate TDHF rotations provide initial points

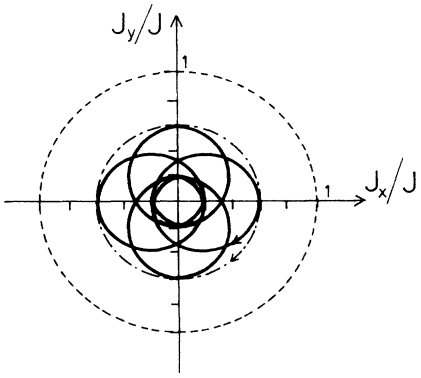

FIG. 9. Same as in Fig. 8 with initial condition on a TDHF rotation at the point $(J_x^0,J_y^0,J_z^0)=J(0.6,0.0,0.8)$.

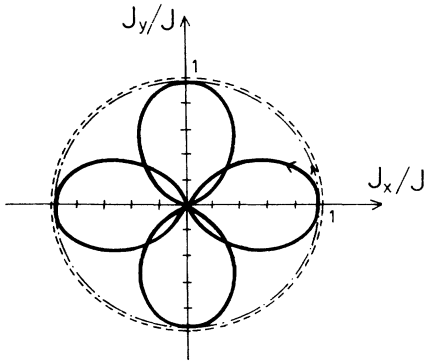

FIG. 10. Same as in Fig. 9 for the initial point $J(0.99,0.0,0.2)$.

with nonzero tangent velocities and with identical energy. This is the case of the initial conditions $J(0.6,0,0.8)$ and $J(0.99,0,0.2)$. The (J_x,J_y) projections of the corresponding trajectories are shown in Figs. 9 and 10, respectively. The patterns are symmetric and periodic in both cases, and one can appreciate the variations of the normal component of the velocity that drives the exact polarization into the sphere. It is seen that the TDHF dynamics is a good reproduction of the exact one during four infinitesimal time steps—those time intervals located one fourth of a period distant from each other—that correspond to those short moments when the exact trajectory lies almost tangent to the sphere. By contrast, in the case displayed in Fig. 8 the four infinitesimal time intervals collapse into four isolated points; thus, the TDHF orbit is a bad approximation to the exact one except for a zero-measure set.

A large number of examples are available; however, due to the difficulties inherent to the nonobvious classification we prefer not to present them in this work. It is clear that no evident systematic exists; as an example, let us quote here that if one chooses a TDHF maximum as an initial condition, the exact trajectories seem to be delocalized in a majority of cases, except when the amount of parity-violating perturbation exceeds some figure that remains to be determined.

VI. SUMMARY AND CONCLUSIONS

In this work we have investigated the many-fermion dynamics generated by an SU(2) Hamiltonian that complements the properties of the general LMG model[1] with those of the parity-violating Hamiltonian in Ref. 19. The TDHF dynamics is especially appealing in the SU(2) frame, and it has been discussed at some length, however not exhausting the variety of Hamiltonians of the adopted general appearance given by Eq. (2.1). Rather than resorting to an analytical or numerical study of the fixed points of the dynamics, we have extensively utilized the geometrical method here proposed that places the emphasis on the shape of the TDHF energy surfaces and the invariant sets determined by their intersections with the Bloch sphere. It is seen that even in complicated situations, i.e., those presented in Sec. IV, such a study is highly useful for predicting characteristics of the phase diagram without performing a numerical integration of the equations of motion. Some applications of this criterion might be the following: (a) the observation that structural instability appears whenever a second-order contact between the energy surface and the Bloch sphere takes place; (b) the observation that degenerate orbits appear when the vertex of the quadrics lies on the J_z axis with $|J_z|>J$; (c) the distinction between rotations and librations according to whether or not the trajectories link the J_z axis; (d) the identification of absolute maxima as tangency points between quadrics and the Bloch sphere; (e) the identification of a saddle point as a tangency point between the sphere and the axis of the hyperboloids, etc.

It follows from the present study that in the general LMG model ($V=W\neq 0, U=0$), whenever both χ_+ and $|\chi_-|$ are above unity, the assertion concerning nondegeneracy of rotations[9] ceases to be valid. This assertion is only true when $W=0$. Moreover, if U does not vanish, the property of librational degeneracy collapses as well. An interesting by-product of the investigation presented here concerns the richness of phase flows taking place in the general LMG model when W is different from zero. Indeed, one should recall that, being the two-body interaction proportional to $\{J_+,J_-\}$ diagonal in the Dicke basis,[1] inclusion of this term in exact or static Hartree-Fock calculations is trivial. The dynamical viewpoint here adopted shows that the TDHF phase portraits are far from trivial and the geometric construction proves its utility in any attempt to classify and qualitatively consider the possible situations.

As a final remark, we would like to mention that an attempt to study and classify the exact trajectories according to the invariant sets where the initial condition belongs on the Bloch sphere should be pursued. This is an interesting task in view of the variety of and in many cases the beauty of the patterns that may appear. We believe that a systematics relating the quality of a TDHF description to the location of the initial wave packet may be, on general grounds, a useful contribution to mean field theory and calculations. In this spirit, a requantization of the TDHF orbits should provide different degrees of approximation to the exact sprectum, and it should be useful as well to examine this subject in future work.

ACKNOWLEDGMENTS

We wish to acknowledge the Programa de Investigaciones de Física del Plasma at our home institution for generous access to their computing facilities. This work was partially performed under Grant 9413d/84 from CONICET and Grant 11473/84 from the Secretaría de Ciencia y Técnica of Argentina.

[1]H. J. Lipkin, N. Meshkov, and A. J. Glick, Nucl. Phys. **62**, 188 (1965); N. Meshkov, A. J. Glick, and H. J. Lipkin, *ibid.*, **62**, 199 (1965); A. J. Glick, H. J. Lipkin, and N. Meshkov, *ibid.* **62**, 211 (1965).
[2]D. Agassi, H. J. Lipkin, and N. Meshkov, Nucl. Phys. **86**, 321 (1966).
[3]A. Arima and F. Iachello, Ann. Phys. (N.Y.) **99**, 253 (1976); **111**, 201 (1978); **123**, 468 (1979).
[4]A. Arima, T. Otsuka, F. Iachello, and I. Talmi, Phys. Lett. **66B**, 205 (1977); **76B**, 139 (1978).
[5]T. Otsuka, A. Arima, and F. Iachello, Nucl. Phys. **A309**, 1 (1978).
[6]S. Levit, Phys. Rev. C **21**, 1594 (1980).
[7]S. Levit, J. W. Negele, and Z. Paltiel, Phys. Rev. C **21**, 1603 (1980).
[8]J. P. Elliot, Physica (Utrecht) **A114**, 1 (1982).
[9]K. K. Kan, P. C. Lichtner, M. Dworzecka, and J. J. Griffin, Phys. Rev. C **21**, 1098 (1980).
[10]R. Gilmore and D. H. Feng, Nucl. Phys. **A301**, 189 (1978).
[11]R. Gilmore and D. H. Feng, Phys. Lett. **85B**, 155 (1979).
[12]K. K. Kan, J. J. Griffin, P. C. Lichtner, and M. Dworzecka, Nucl. Phys. **A332**, 109 (1979).
[13]K. K. Kan, Phys. Rev. C **22**, 2228 (1980).
[14]P. Kramer and M. Saraceno, *Geometry of the Time-Dependent Variational Principle in Quantum Mechanics* (Springer-Verlag, Berlin, 1981).
[15]D. H. Feng and R. Gilmore, Phys. Rev. C **26**, 1244 (1982).
[16]S. T. Belyaev and I. M. Pavlichenkov, Nucl. Phys. **A388**, 505 (1982).
[17]H. G. Solari and E. S. Hernández, Phys. Rev. C **26**, 2310 (1982).
[18]H. G. Solari and E. S. Hernández, Phys. Rev. C **28**, 2472 (1983).
[19]D. M. Jezek, E. S. Hernández, and H. G. Solari, Phys. Rev. C **34**, 297 (1986).
[20]S. M. Abecasis, A. Faessler, and A. Plastino, Z. Phys. **220**, 88 (1969).
[21]E. S. Hernández and A. Plastino, Lett. Nuovo Cimento **3**, 601 (1972).
[22]F. T. Arecchi, E. Courtens, R. Gilmore, and H. Thomas, Phys. Rev. A **6**, 2211 (1972).
[23]R. Gilmore, Rev. Mex. Fis. **C3**, 417 (1971).